Ironless Axial Flux Wind Turbine Motor with Two Cylindrical Magnet Rings

M. Bonnet, Jean-François Llibre, D. Harribey, Y. Lefevre

Ironless Axial Flux Wind Turbine Motor with Two Cylindrical Magnet Rings

M. Bonnet, J. F. Llibre, D. Harribey, Y. Lefèvre
LAPLACE, UNIVERSITY OF TOULOUSE, CNRS, INPT, UPS, TOULOUSE, FRANCE,
EMAIL: {MBONNET, LLIBRE, DOMINIQUE.HARRIBEY, YVAN.LEFEVRE}@LAPLACE.UNIV-TLSE.FR

***Abstract* --An ironless axial flux wind turbine motor is presented in this paper. The aim of this paper is to propose a motor that can be manufactured from simple components: magnets, copper and plastic. The motor must be feasible even in remote areas where machining facilities are limited. The winding and mechanical supports are sized from the magnets. The motor is therefore designed to be simple to reproduce and affordable in terms of manufacturing costs. Two rows of magnets are used to improve the performance of the motor. During design, choices on dimensions were made with fast calculations of output performance using models developed specifically for ironless motors. The performance measured on the prototype is in perfect agreement with the finite element simulations and the proposed models.**

***Index Terms*—Axial flux machine, Additive manufacturing, Permanent magnet motor, Wind power generation**

I. INTRODUCTION

RENEWABLE energies are very interesting sources of energy for isolated areas. It allows these distant areas to charge batteries and then to provide them electricity ready to use. WindAid [1] aims to allow remote areas of Peru to generate their own electrical energy. The targeted zones are very windy, so the creation of a complete wind turbine is planned with the possibility of manufacturing it on site. All components of the wind turbine and its electrical connection shall be manufactured, assembled and/or purchased locally. In this context, a motor is presented in this article to meet these needs.

Axial Flux Permanent Magnet Motors (AFPM) have already been used for power generation from wind turbines. The interest of these machines is that they generally have a higher power density than their radial flux equivalent [2]. AFPMs are also interesting because they can be used in direct connection to the wind turbine [3] which limits the losses by removing the gear box.

Different topologies of axial flux motors exist depending on the number of rotor and stator used. A structure with two rotors and one stator is preferred to maximize the magnetic field on the coils. In this structure, the iron in the stator is not mandatory [4]. Still on this structure, it is possible to use Halbach array magnets [5]. This allows the magnetic fields on the stator to be canalized even further. The flux lines of the magnets intrinsic to this structure make iron optional on the rotors. However, the cost and difficulties in assembling these magnets make this technology difficult to consider for a motor manufactured in a remote area. A structure with two stators and one rotor is chosen to limit the mechanical stresses on the rotor, to facilitate the cooling of the stators and to ensure continuity of operation even with a damaged stator [6]. In this structure, the rotor can be ironless while keeping very good performance [7].

The black spot of AFPM is the manufacturing of the iron lamination of the ferromagnetic sheets [8]. The present topologies allow the removal of iron but still have it on one of their parts. The YASA topology is an interesting alternative [9] but remains difficult to manufacture locally in remote areas. Ironless motors are the simplest to manufacture because they do not require laminations or Soft Magnetic Composites (SMC) [10]. However, this motor has lower performances due to the non-canalization of the magnetic field. To have interesting performances, the air gap must be as small as possible. In the topology with two rotors and a central stator, depending on the number of winding layers, the air gap can be increased [11]. The structure with two stators and one rotor is therefore preferred. This also limits the mechanical attraction forces between two rotors.

On AFPM, several shapes of magnets can be used. This will have an impact on the performance and shape of the electromotive forces (EMFs) [12]. Tile-shaped magnets are most often used to maximize the area of magnet covering the energized conductors [12]. However, parallelepiped magnets [5] or cylindrical magnets [3][13] can be used for cost or assembly reasons.

Next references indicate from equations, how to choose the dimensions of an AFPM with iron [7][14] or without [5][15] for a wind turbine. The purpose of this article is to size an ironless axial flux motor from the dimensions of preselected magnets. Cylindrical magnets are chosen for their availability (easy to find on the shelves), cost and ease of assembly. To compensate for the lack of conductor coverage, a second ring of magnets is suggested. The coils and the stators are identical in shape and design. All the proposed coils are manufactured and assembled in exactly the same way. The main goal of this article is the reproducibility of the proposed motor topology. The motor performance is calculated from the dimensions imposed by the selected magnets and corresponding coils. Methods specifically developed for ironless motors [16] are used to calculate the output performance. There are then validated by 3D Finite Element Analysis (FEA) methods and experimental measurements.

II. MOTOR DESCRIPTION

This generator must provide an electrical power of 200W at 2000rpm to a 24V battery. The generator is driven in

rotation by the wind turbine whose average speed is around 700rpm. It is necessary to have a gear ratio of about 3.

The design of the proposed motor is above all thought to be as simple as possible to manufacture and to limit manufacturing costs. To avoid iron machining, the motor has no iron in the stator and rotor. The magnets are cylindrical and can be found on shelves. The coils are all identical. Motors without iron have electromagnetic performances much lower than their equivalent with iron. Choices on coils and magnets are therefore made to try to compensate for the absence of iron. The magnets chosen on the shelves are the starting point of the sizing.

To give a correct idea of our approach, the final design of the prototype is shown in Fig. 1. The following explain all the choices done.

Fig. 1. Prototype of the wind turbine axial flux motor

A. Magnets

To maximize the magnetic field with an axial flux motor, trapezoidal magnets are most commonly used for these motors. However, these forms of magnets are expensive. They are even more expensive if the magnets are custom made. Cylindrical magnets were therefore chosen to reduce costs. However, the shape of these magnets does not cover as much of the active part as the tile-shaped magnets. To have more active parts in the field of these magnets, a second magnet is added on the same pole (Fig. 2). The same active part is covered by two magnets of the same polarization.

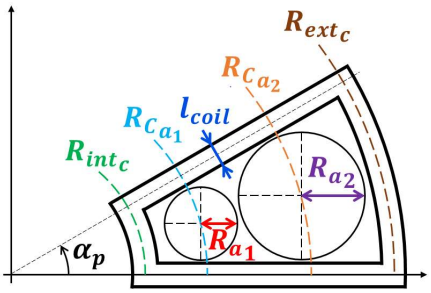

Fig. 2. Magnets and a winding on one pole

B. Windings

The dimensions of the active parts are determined from the magnets. These coils must be larger than the two magnet diameters and the space between them.

To maximize the output torque, the radius of the motor is chosen to be large. What limits the maximum size of this radius is the material used for the mechanical supports. The mounts must be able to withstand the forces involved without mechanical deflection. In addition, when manufacturing these supports, care must be taken to ensure that the air gap is constant across the plane. With 3D printing of PA 2200HD [18], these mechanical properties and accuracy are ensured for radii of less than 8cm.

To facilitate winding, the coils should not overlap. The Factional Slot Concentrated Windings (FSCW) type is preferred. This type of winding allows to limit the coil heads, and thus to limit the Joule losses [19]. But it creates more eddy current losses in the magnets and the rotor iron. This is not a problem for a motor without iron, only the copper and magnet losses remain. This winding imposes a trapezoidal shape of the coils (Fig. 2).

The inner radius of the coils is defined by the coil heads on this radius. It must be possible to twist the wires without problems. This also depends on the diameter of the conductors and the thickness of the slots. The diameter of the conductor is chosen so that for a current I of 1A, the current density J corresponds to 5A/mm². The wire diameter is therefore 0.5mm. An FSCW can reach a filling factor k_{fill} of 0.5. To maximize the filling factor, the width of the coil is chosen as a multiple of the wire diameter, here this width l_{coil} is 4mm.

The height of the coils should not be too high because the magnetic field is not channeled and therefore cannot reach conductors too far from the magnets. A height of 7mm is considered relevant for the performance but also for the manufacturing. A coil that is too thin is more complex to manufacture.

The number of conductors $n_c = 70$ is deduced from:

$$JS_{coil}k_{fill} = n_c I \tag{1}$$

The internal radius R_{int_c} of the coils is then in turn imposed by these parameters. The number of coils in a stator must therefore take into account the angle α_{coil} of the coil which is related to the number of pole pairs p (Fig. 2).

For more reproducibility, the two stators must be identical and produce the same EMFs. In order for the coils to see an identical flux generated by the magnets when the rotor rotates, there is no mechanical angular shift between the two stators. All the coils are wound in the same direction and in the same way, and the coils of the same phase of two different stators are connected in parallel.

C. Manufacturing

The motor performance is calculated by a dedicated model and by 3D FEA. If the calculated performance is lower than expected, it is necessary to choose larger magnets but also to adapt the size of the coils to these new magnets. Then the performance must be recalculated until the expected values are reached.

With the stator and rotor dimensions chosen previously, it is possible to have 12 cylindrical magnets on the rotor and 9 coils on a stator. The main dimensions of the active parts are summarized in Table I.

TABLE I
PARAMETERS OF THE ACTIVE PARTS OF THE PROPOSED PROTOTYPE

Rotor $j = 1$: Inner ring $j = 2$: Outer ring	R_{a_1}	6 mm
	R_{a_2}	11 mm
	$R_{c_{a_1}}$	31 mm
	$R_{c_{a_2}}$	49 mm
	Axial length h_a	12 mm
	p	6
	α_p	π/p
	J_r	1.192 T
	μ_{r_a}	1.026
	Magnetization	N35 [20]
Stator	R_{int_c}	22 mm
	R_{ext_c}	63 mm
	Axial length h_{coil}	7 mm
	l_{coil}	4 mm
	Conductor diameter	$\emptyset$ 0.5mm
	n_c	70
	k_{fill}	0.491
	$n_{coil/stator}$	9

The complete manufacturing of this prototype is available in video online [17]. The mechanical supports of the stators, made of non-active materials, are identical. These supports are made here by additive manufacturing PA 2200 HD [18]. This makes it possible to manufacture these motor parts quickly and accurately. It is possible to use other non-magnetic materials to reduce the price, such as wood. It must be ensured that the material chosen can mechanically withstand the speeds at which the rotor must rotate. The magnets are glued to this support at their dedicated locations. Ball bearings are then added to the non-active supports.

The non-active supports have a free shape. However, they must ensure that the active parts are held in place mechanically. The shapes printed for the prototype of this article can be adapted or modified.

III. CHARACTERIZATION AND FINAL SIZING

A. *Open circuit magnetic field calculation*

To calculate the performance of this motor before and during its design phase, a field calculation model is used [16]. This model allows to quickly know the open circuit magnetic field of the motor whatever the geometry of the magnets and conductors. From a single magnet, the total open circuit magnetic field created by several identical magnets is calculated.

By considering several magnets identical in shape and magnetization but located at different places in space, the field produced by these different magnetic field sources at a single target point C is identical to the sum of the magnetic field produced by a single magnet at several target points. Each of these target points is the unique target point in the reference frame associated with each magnet (Fig. 3).

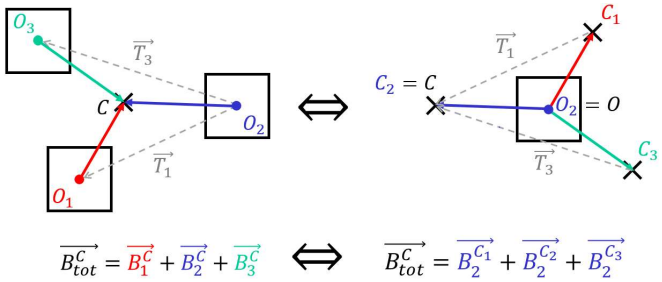

Fig. 3. Recomposition of the magnetic field produced by three magnets from the field produced by a single magnet

Let be a target point C where the open circuit magnetic field of the rotor must be calculated. The vectors (2) are used to represent the position of the point C in the reference frame associated with each rotor magnet. The index j indicates whether the magnet belongs to the inner or outer ring (Table I):

$$\overrightarrow{OC_k^j} = \overrightarrow{OC} - \overrightarrow{T_k^j} \tag{2}$$

To calculate the total open circuit magnetic field, two reference magnets must be used, one for each ring of the rotor. These reference magnets are positioned at the center of the cylindrical reference frame. To recompose the open circuit field from these magnets, it is necessary to reposition the necessary target points in the reference frame of these reference magnets (Fig. 3). For this purpose, two translation vectors are defined, one per reference magnet (3).

$$\overrightarrow{T_k^j} = \left[R_z(\alpha_p)\right]^{k-1}\left(R_{c_{a_j}} \quad 0 \quad 0\right)^{\mathrm{T}} \tag{3}$$

With $\left[R_z(\alpha_p)\right]$ the rotation matrix around the z-axis by an angle α_p, k the number of the magnet ranging from 1 to $2p$ in this case and $R_{c_{a_j}}$ the radius of the center of the magnets (Table I and Fig. 2). The total flux magnetic density of the rotor can then be calculated from the field of the two reference magnets B_0^1 and B_0^2.

$$\overrightarrow{B_{tot}^c} = \sum_{k=1}^{2p} (-1)^{k-1}\left(\overrightarrow{B_0^{1\,C_k^1}} + \overrightarrow{B_0^{2\,C_k^2}}\right) \tag{4}$$

With (4), the open circuit magnetic field of the rotor can be calculated at any point C in space. Only the knowledge of the field of the two reference magnets and the geometrical position of the magnets on the rotor are necessary.

B. *Calculation of the static torque and FEM*

For an ironless motor, it is sufficient to use the Lorentz force law to calculate the static torque. The torque is calculated in the rotor reference frame as in [10].

$$C_{rotor} = -\iiint_{V_{coils}} \left(\vec{J}(\vec{r}.\vec{B}) - \vec{B}(\vec{r}.\vec{J})\right) \cdot \overrightarrow{e_z} dV_{coils} \tag{5}$$

The positions of the active parts at each instant of the rotation define new target points where the total flux magnetic density is calculated with (4). The active parts of conductors are only in the radial direction, so only the axial component of the field B_z and the radial constant current density J_r create a useful torque.

$$C_{stc} = J_r \iiint_{V_{coils}} rB_z dV_{coils} \quad (6)$$

The conductors can be assimilated to a wire if the open circuit magnetic field is uniform in the coil volume. This can be the case for the motor topology with two rotors [10][16]. For other ironless motor topologies, such as the prototype of this article, the open circuit magnetic field changes from nothing to everything in the volume of the coils. Thus, in order to have a relevant torque calculation whatever the topology of the motor adopted, the volume integral is preferred. The volume integral (6) is developed according to r. The volume element can be expressed: $dV_{coil} = dS_{sc}dr$. Where S_{sc} is cross-section of the coil of normal $\overrightarrow{e_r}$:

$$C_{stc} = J_r \int_{R_{int_c}}^{R_{ext_c}} \left(\iint_{S_{cs}} rB_z(r,\theta,z)\, dS_{cs} \right) dr \quad (7)$$

The surface integral of (7) is associated with a conductor section at a given radius. The open circuit magnetic field is evaluated at four Gauss points distributed over a coil section S_{sc} (Fig. 4.a). The surface integral is calculated numerically by the Gauss-Legendre method. The calculation of this surface integral for several radii allows to know the function to integrate according to the radius (Fig. 4. b). This line integral is calculated by the trapezoid method. For a given position of an active part, for 100 different sections and 4 points per section, 4x100 different target points are needed.

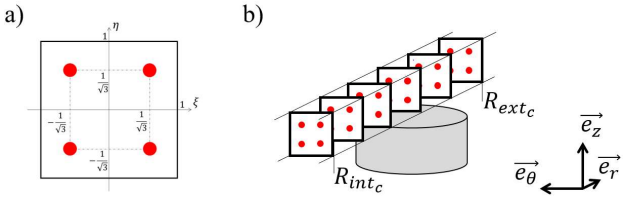

Fig. 4. a) Gauss points to calculate the surface integral
b) Distribution of coil sections of a conductor above a permanent magnet to calculate the line integral

As this motor has smooth poles, the static torque of a phase is the image of the EMF of this same phase (8) with a constant current I.

$$e = \frac{C_{stc}\Omega}{I} \quad (8)$$

Calculating the EMF with this method allowed to quickly study the performances of the prototype during its design, in particular on the height of the coils. Indeed, the magnetic field in vacuum decreases rapidly in intensity with distance. Thus, having a coil too high is not relevant because the conductors farthest from the magnets are only slightly bathed in the magnetic field.

C. 3D finite elements calculation

To validate the dimensions and performances announced by the model, a 3D numerical simulation is performed on ANSYS Maxwell. The stator and one rotor are represented in full. As the two rotors are identical and connected in parallel, only one is needed to calculate the FEMs and the static torques (Fig. 5). The magnets are placed in a bearing strip. The magnets are moved during the transient simulation on a pair of mechanical poles. Since the motor is ironless, the air box is large enough to consider the magnetic field to be zero at the outer surfaces.

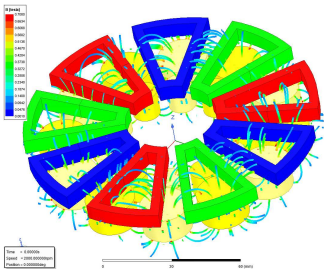

Fig. 5. Motor simulated on ANSYS Maxwell with some induction magnetic field lines displayed

The calculation of the torque by ANSYS on this type of motor is inaccurate if a large number of mesh elements is not used. It is possible to quickly calculate the load torque by a no-load simulation without using too many mesh elements. By calculating the no-load fluxes of the coils and by derivation, we obtain the EMFs and then the torque according to (8).

D. Winding type

With the number of magnets and coils defined in part II, it is possible to describe several types of windings. The winding is defined for one stator and is reproduced identically on the second stator. The slots and teeth on this ironless motor are defined as in Fig. 6. There are two coils in the same slot, so it is a double layer winding.

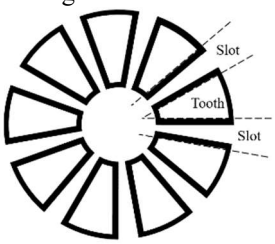

Fig. 6. Definition used for "slots" and "teeth" of the ironless stator

The number of poles pair p can be 1, 2, 3 or 6; which corresponds to NNNN-SSSS, NNN-SSS, NN-SS and N-S magnets respectively. To define these windings, [21] is used for this motor with Q the number of slots, Q_m the number of slots per phase, q the number of slots per pole and per phase and m the number of phases (Table II).

The winding for $p = 1$ is not retained because it is a distributed type winding ($q > 1$) which implies an overlap of the coil heads. To choose the winding among the three other possibilities, the EMFs are calculated theoretically. The winding that generates the least amount of harmonics on these EMFs is the selected winding. According to Fig. 7, the solution with $p = 6$ is therefore the selected winding.

TABLE II
WINDING PARAMETERS

m	Q	p	Q_m	q	$t = \gcd(Q,p)$	$Q_t = Q/t$
3	9	1	3	3/2	1	9
3	9	2	3	3/4	1	9
3	9	3	3	1/2	3	3
3	9	6	3	1/4	3	3

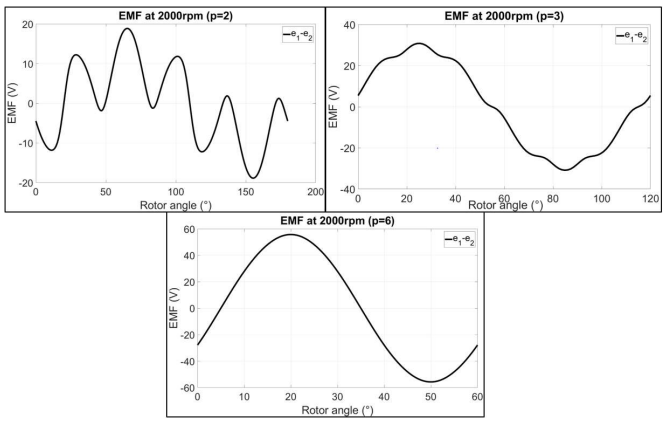

Fig. 7. Phase to phase EMF for three different values of p

E. *Interest of the two magnet rings*

With the length of the active part of the conductors, it is interesting to observe the contribution of this second magnet ring. Fig. 8 shows the calculated static torque generated by each magnet ring for a current of 1A in the coils. The small ring contributes to the creation of 20% of the total torque. With a current of 1A, the torque is 151.5mN.m for a mass of active parts of 830.8g. The torque per unit of mass is then 0.182N.m/kg. If only the outer ring is kept with the inner radius R_{int_c} of the coils adapted to this only ring, the torque for 1A is 119mN.m. For a mass of active parts of 676.3g. The torque per unit of mass is therefore 0.176N.m/kg, which is slightly lower than that with two rings.

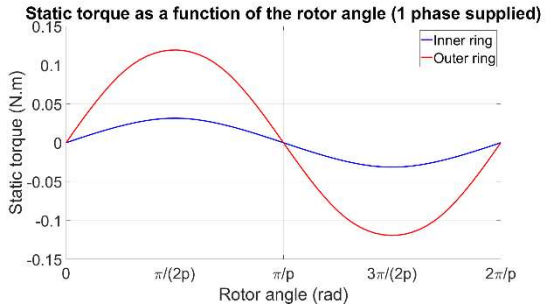

Fig. 8. The calculated static torque for one phase supplied with 1A

With the calculation model it is possible to compare the theoretical EMFs of this prototype with what it would have given with trapezoid magnets. In order for the magnets to operate with the same winding, the dimensions of the trapezoidal magnets used are defined from the dimensions of the cylindrical magnets (Fig. 9) and (9), (10) and (11). Both types of magnets have the same height of 12 mm.

$$R_{ext_t} = R_{C_{a_2}} + R_{a_2} \tag{9}$$

$$R_{int_t} = R_{C_{a_1}} - R_{a_1} \tag{10}$$

$$\alpha_t = 2\sin^{-1}\frac{R_{a_2}}{R_{C_{a_2}}} \tag{11}$$

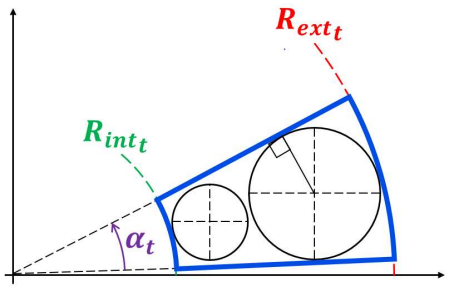

Fig. 9. Trapezoid magnet (blue) sized from cylindrical magnets (black)

The open circuit magnetic field is also recomposed with the method used in [16]. This time, the reference magnet is merged with one of the rotor magnets. The relative position of the magnets to this reference magnet is found with the rotation matrix. The position of the new target points for the trapezoid magnets are found with:

$$\overrightarrow{OC_k} = \left[R_z(\alpha_p)\right]^{-k}\overrightarrow{OC} \tag{12}$$

The total magnetic flux density of the rotor can then be calculated from the field of the reference magnet B_0^1:

$$\overrightarrow{B_{tot}^c} = \sum_{k=0}^{2p-1}(-1)^k\left[R_z(\alpha_p)\right]^k\overrightarrow{B_0^{1C_k}} \tag{13}$$

The EMFs as a function of the magnet shapes are given in Fig. 10.

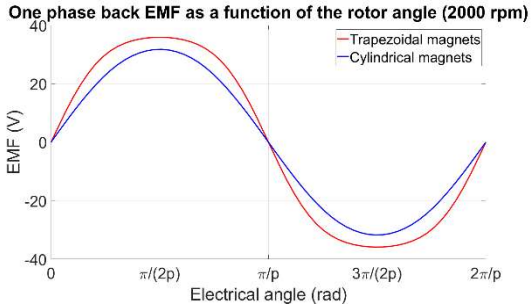

Fig. 10. Theoretical one phase EMF at 2000 rpm

The maximum amplitude goes from 35.89V with trapezoidal magnets to 31.74V with cylindrical magnets. This means a 12.6% decrease in motor output performance. But switching from trapezoidal to cylindrical magnets reduces the magnet mass by 26.8%. So the torque density remains interesting even with cylindrical magnets. Moreover, the cost of cylindrical magnets is much lower than the trapezoidal magnets used here. The EMF of cylindrical magnets is closer to a sine than that of trapezoidal magnets. The shape of these curves was obtained without optimization.

IV. Experimental Measurements

This ironless axial flux motor, used in generator operation in the WindAid project, has two special features (Fig. 1):

- two magnet rings with $p = 6$,
- an identical FSCW on both stators, with $Q = 9$.

To match the output voltage to the voltage of the battery to be supplied, the delta coupling is chosen (Fig. 11).

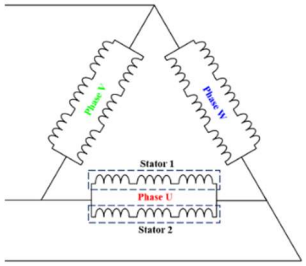

Fig. 11. Coupling of the coils of the wind turbine motor

A. *Measurement of EMFs*

The EMFs are measured in open circuit. Fig. 12 shows the EMF waveform with one stator and the rotor rotated by hand. To validate the model, the motor shaft is mounted on a drilling machine that rotates it at constant speed. The measured EMFs are compared to the voltages calculated by ANSYS and the model in Fig. 13.

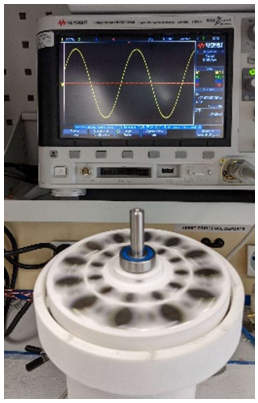

Fig. 12. Line to line EMF measured for one stator at 330 rpm

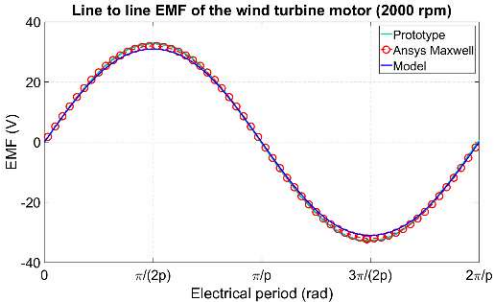

Fig. 13.Comparison of EMFs

The model gives an amplitude of 31.74V, 32.00V predicted by ANSYS-Maxwell and 32.97V measured on the prototype. The electrical frequency measured with the oscilloscope is 200Hz.

B. *Measurement of static torque*

A single phase of a single stator is supplied with a direct current I_{DC}. For this purpose, the coupling of the motor is undone and the static torque is measured for each phase separately (Fig. 14 a).

The motor is then rotated at very low speed to avoid any transient phenomenon (such as eddy current or hysteresis losses in the magnets). The force developed by the interaction between the open circuit magnetic field and the coils is measured by a force sensor. With the knowledge of the lever arm, i.e. the distance of the sensor from the center of the motor, the torque can be deduced from the measured force (Fig. 14 b). The speed of rotation is slow enough to consider that each position of the rotor is at a static position. The measured force is directly the Laplace force developed between the magnets and the coils (10).

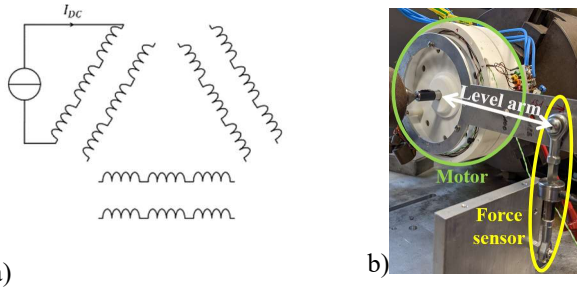

a) b)

Fig. 14. a) Coupling and power supply used for static torque tests
b) The prototype on the static torque test bench

The amplitude of the static torque for a DC current of 2A is 303.1mN.m by the model, 309.7mN.m by 3D FEA and 330 mN.m measured on the prototype (Fig. 15). The models remain in agreement with the measurements on prototype even if the differences are slightly larger than with the EMF.

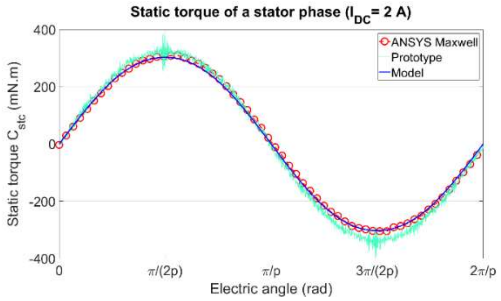

Fig. 15. Comparison of static torques calculated theoretically, by ANSYS and measured

C. *Tests with rectifier and load resistance*

For the load tests, the motor is maintained at a constant speed by a drill (Fig. 16). The torque of the motor is measured by the help of a force sensor. The motor is connected to a voltage rectifier and a load resistance (Fig. 17).

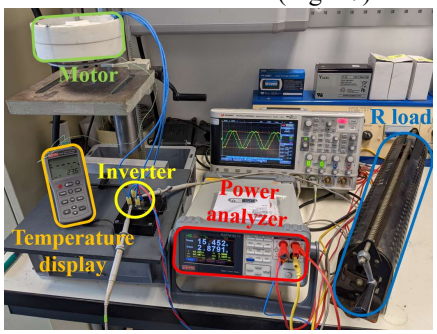

Fig. 16. Motor connected to a rectifier and a load resistance

A power meter is connected to the output of the rectifier to measure the electrical power output. The mechanical input power is calculated from the motor speed and the torque developed. The efficiency of the motor and rectifier assembly can therefore be calculated.

With a speed of 2207.8rpm and a torque of 1.306N.m, the mechanical power is 302W. The measured electrical power given to the load resistance is 216W. The efficiency of the

generator with the rectifier is therefore 71.5%. This torque corresponds, according to the model, to a 2A rms in a coil. Considering only the Joule losses and an efficiency of 90% for the rectifier, the theoretical efficiency is 76.5%.

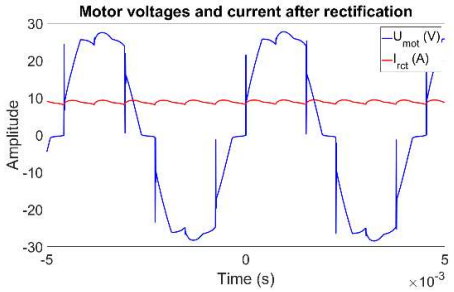

Fig. 17. Line to line voltage before rectification, current after rectification

V. CONCLUSION

This article proposes the simplified design of a completely ironless axial flux motor. The main purpose is to guide the choice of the geometrical dimensions around the magnets composing the rotor. These magnets are selected for their price and their availability on the market. A second magnet ring is proposed to improve the output performances. A dedicated model validated by FEA 3D allows the selection and sizing of all active parts of the motor.

Compared to trapezoidal magnets, the cylindrical magnets used have a slightly lower performance but a much lower mass and cost. The proposed prototype can be manufactured on site in remote areas. It allows to have more than 200W electric with an interesting efficiency. Several motors of this type can be associated on the same wind turbine to reinforce the electric power produced. The voltages produced are almost perfect sine, which can be interesting for the rectifier. It should be noted that this ironless motor has a low inductance, due to the absence of iron. To make high power motor, stronger magnets must be chosen. The materials of mechanical supports will then have to withstand the pressure involved. The increase in power is limited by the technology of materials used.

VI. REFERENCES

[1] WindAid Institute, 2022. [Online] https://www.windaid.org

[2] Parviainen, A., Pyrhonen, J., & Kontkanen, P. (2005, May). Axial flux permanent magnet generator with concentrated winding for small wind power applications. In *IEEE International Conference on Electric Machines and Drives, 2005.* (pp. 1187-1191). IEEE.

[3] Ferreira, A. P., Silva, A. M., & Costa, A. F. (2007, September). Prototype of an axial flux permanent magnet generator for wind energy systems applications. In *2007 European Conference on Power Electronics and Applications* (pp. 1-9). IEEE.

[4] Price, G. F., Batzel, T. D., Comanescu, M., & Muller, B. A. (2008, November). Design and testing of a permanent magnet axial flux wind power generator. In *Proceeding of the 2008 IAJC-IJME International Conference* (pp. 17-19).

[5] Subotic, I., Gammeter, C., Tüysüz, A., & Kolar, J. W. (2018). Weight Optimization of Coreless Axial-Flux PM Machines. *IET Electric Power Applications*.

[6] Djebarri, S., Charpentier, J. F., Sculiller, F., & Benbouzid, M. (2015). Design and performance analysis of double stator axial flux PM generator for rim driven marine current turbines. *IEEE Journal of Oceanic Engineering*, *41*(1), 50-66.

[7] Javadi, S., & Mirsalim, M. (2009). Design and analysis of 42-V coreless axial-flux permanent-magnet generators for automotive applications. *IEEE Transactions on Magnetics*, *46*(4), 1015-1023.

[8] Gieras, J. F., Wang, R. J., & Kamper, M. J. (2008). *Axial flux permanent magnet brushless machines*. Springer Science & Business Media.

[9] Woolmer, T. J., & McCulloch, M. D. (2007, May). Analysis of the yokeless and segmented armature machine. In *2007 IEEE International Electric Machines & Drives Conference* (Vol. 1, pp. 704-708). IEEE.

[10] Bonnet, M., Lefèvre, Y., Llibre, J. F., Harribey, D., Defaÿ, F., & Sadowski, N. (2019, August). 3D magnetic field model of a permanent magnet ironless axial flux motor with additively manufactured non-active parts. In *2019 19th International Symposium on Electromagnetic Fields in Mechatronics, Electrical and Electronic Engineering (ISEF)* (pp. 1-2). IEEE.

[11] Yao, W. S., Cheng, M. T., & Yu, J. C. (2020). Novel design of a coreless axial-flux permanent-magnet generator with three-layer winding coil for small wind turbines. *IET Renewable Power Generation*, *14*(15), 2924-2932.

[12] Radwan-Praglowska, N. (2018, June). Impact of permanent magnets shape and arrangement for selected parameters in coreless axial flux generator. In *2018 International Symposium on Electrical Machines (SME)* (pp. 1-6). IEEE.

[13] Fei, W., Luk, P. C. K., & Jinupun, K. (2010). Design and analysis of high-speed coreless axial flux permanent magnet generator with circular magnets and coils. *IET electric power applications*, *4*(9), 739-747.

[14] Bumby, J. R., Martin, R., Mueller, M. A., Spooner, E., Brown, N. L., & Chalmers, B. J. (2004). Electromagnetic design of axial-flux permanent magnet machines. *IEE Proceedings-Electric Power Applications*, *151*(2), 151-160.

[15] Batzel, T. D., Skraba, A. M., & Massi, R. D. (2014). Design and test of an ironless axial flux permanent magnet machine using a halbach array. *International Journal of Modern Engineering*, 52.

[16] Bonnet, M., Lefèvre, Y., Llibre, J. F., Harribey, D., & Defay, F. (2021). Model of an ironless axial flux permanent magnet motor based on the field produced by a single magnet. *IEEE Transactions on Magnetics*, *57*(7), 1-4.

[17] D. Harribey, *3D printed alternator for micro-wind turbine*, (July 22, 2021). [Online] https://www.youtube.com/watch?v=rXIE20B66dw

[18] Initial Design & Production Prodways. [Online]. https://www.initial.fr/materiaux/matieres-plastiques/poudres-polyamide/

[19] De Donato, G., Capponi, F. G., Rivellini, G. A., & Caricchi, F. (2012). Integral-slot versus fractional-slot concentrated-winding axial-flux permanent-magnet machines: comparative design, FEA, and experimental tests. *IEEE Transactions on Industry Applications*, *48*(5), 1487-1495.

[20] HKCM. [Online]. https://www.hkcm.de/desk.php/

[21] Bianchi, N., & Dai Prè, M. (2006). Use of the star of slots in designing fractional-slot single-layer synchronous motors. *IEE Proceedings-Electric Power Applications*, *153*(3), 459-466.

VII. BIOGRAPHIES

M. Bonnet was graduated from ENSEEIHT of Toulouse, France, in electrical engineering in 2018 and received the Ph.D. degree in electrical engineering from National Polytechnic Institute of Toulouse in 2021. He is actually a post-doctoral fellow specializing in the modeling of electrical machines at the Plasma and Energy Conversion Laboratory (LAPLACE), Toulouse.

J. F. Llibre has received the Ph.D. degree in Electrical Engineering from National Polytechnic Institute of Toulouse in 1997. He is assistant professor since 1998 and teaches electrical engineering in the University Institute of Technology of Blagnac near Toulouse since 2003. He joined the GREM3 electrodynamics research group of LAPLACE laboratory in 2010. His field of interest is related to the modeling and the sizing of electrical machines.

D. Harribey was born in 1959 in Toulouse, France. He is now a CNRS research engineer in LAPLACE laboratory. He is in charge of the electromechanical study, design and testing of electric actuator prototypes developed by the GREM3 research group. He was awarded the CNRS Crystal Medal in 2016.

Y. Lefevre was graduated from ENSEEIHT of Toulouse, France, in electrical engineering in 1983 and received the Ph.D. degree from National Polytechnic Institute of Toulouse in 1988. He is currently working as a CNRS Researcher at the GREM3 research group of LAPLACE laboratory. His field of interest is the modeling of coupled phenomena in electrical machines in view of their design